

# The effect of Zr-substitution in $\text{La}_{1-x}\text{Sr}_x\text{Co}_{0.2}\text{Mn}_{0.6}\text{Zr}_{0.2}\text{O}_{3-\delta}$ ( $M = \text{Fe}, \text{Mn}$ ) on the crystal structure, thermal expansion and electronic transport properties



Vegar Øygarden\*, Tor Grande

Department of Materials Science and Engineering, NTNU Norwegian University of Science and Technology, NO 7491 Trondheim, Norway

## ARTICLE INFO

### Article history:

Received 5 September 2016

Received in revised form 5 January 2017

Accepted 16 January 2017

Available online xxx

### Keywords:

Perovskite

Zr-substitution

X-ray diffraction

Electrical conductivity

Thermal expansion

## ABSTRACT

The effect of Zr-substitution on the evolution of crystal structure, thermal expansion and the electronic transport properties is reported for  $\text{La}_{1-x}\text{Sr}_x\text{Co}_{0.2}\text{Fe}_{0.6}\text{Zr}_{0.2}\text{O}_{3-\delta}$  ( $0.1 \leq x \leq 1.0$ ) and  $\text{La}_{1-x}\text{Sr}_x\text{Co}_{0.2}\text{Mn}_{0.6}\text{Zr}_{0.2}\text{O}_{3-\delta}$  ( $x = 0.1, 0.2, 0.25, 0.3$ ).  $\text{La}_{1-x}\text{Sr}_x\text{Co}_{0.2}\text{Fe}_{0.6}\text{Zr}_{0.2}\text{O}_{3-\delta}$  was found to be single-phase for the compositions investigated. The electrical conductivity of  $\text{La}_{1-x}\text{Sr}_x\text{Co}_{0.2}\text{Fe}_{0.6}\text{Zr}_{0.2}\text{O}_{3-\delta}$  demonstrated a maximum for  $x = 0.5$ , while the area specific resistance was shown to decrease significantly with increasing Sr-content due to an increased concentration of oxygen vacancies. No signs of oxygen vacancy ordering were observed. The area specific resistance of  $\text{La}_{0.3}\text{Sr}_{0.7}\text{Co}_{0.2}\text{Fe}_{0.6}\text{Zr}_{0.2}\text{O}_{3-\delta}$  at 600 °C is close to an order of magnitude lower than reported values for  $\text{La}_{0.4}\text{Sr}_{0.6}\text{Co}_{0.2}\text{Fe}_{0.8}\text{O}_{3-\delta}$ . The series  $\text{La}_{1-x}\text{Sr}_x\text{Co}_{0.2}\text{Mn}_{0.6}\text{Zr}_{0.2}\text{O}_{3-\delta}$  was found as multiphase materials. The stability of both series is discussed with respect to the red-ox properties of the transition metals.

© 2017 Elsevier B.V. All rights reserved.

## 1. Introduction

Intermediate temperature solid oxide fuel cells (IT-SOFC) have received significant attention in recent years as the search for green energy converters has become more relevant. Lower operating temperature allows the use of metallic interconnects, whilst also improving material compatibility and sealing [1]. The development of these fuel cells is limited due to the lack of efficient cathode materials at lower operating temperatures [2]. New materials which combine high electronic and ionic conductivity with chemical phase stability, high catalytic activity for oxygen reduction, and moderate thermal expansion are of high scientific and technological interest.

$\text{La}_{1-x}\text{Sr}_x\text{Co}_{1-y}\text{Fe}_y\text{O}_{3-\delta}$  has been extensively investigated as a potential cathode material in SOFCs [3–7]. Both the ionic and electronic conductivity is shown to increase with increasing Sr-content due to the formation of electron holes and oxygen vacancies [5]. The ionic conductivity reaches a maximum for Sr-content equal to ~0.5. For high Sr-concentrations it is reported that the oxygen vacancies order and form defect clusters, which severely reduces the ionic conduction due to an increased activation barrier for ionic transport [8–10].

In perovskites, B-site substitution of high valence cations such as  $\text{Zr}^{4+}$ ,  $\text{Nb}^{5+}$  and  $\text{Ta}^{5+}$  has been shown to increase structural stability whilst simultaneously reducing thermal expansion [11,12]. These cations bond strongly to their surrounding oxygen sites due to the high

and stable valence state, which results in short bond-length thereby inducing local structural perturbations of the perovskite  $\text{BO}_6$  octahedra. These distortions are suggested to prevent long-range ordering of oxygen vacancies which could inhibit defect clustering. Retaining high vacancy concentration, whilst simultaneously avoiding vacancy ordering is crucial in order to achieve a high rate of oxygen ion diffusion.

$\text{Zr}^{4+}$ ,  $\text{Nb}^{5+}$  and  $\text{Ta}^{5+}$  have no d-electrons, and will therefore not contribute to the electronic conductivity, however, the highly stable oxidation states enables tuning of the oxidation states of other B-cations through the effect of electroneutrality. This in turn makes it possible to optimize the electronic properties.

Here we report on the crystal structure, electrical transport and thermal expansion in the solid solution series of  $\text{La}_{1-x}\text{Sr}_x\text{Co}_{0.2}\text{Fe}_{0.6}\text{Zr}_{0.2}\text{O}_{3-\delta}$  ( $0.1 < x < 1.0$ ) and  $\text{La}_{1-x}\text{Sr}_x\text{Co}_{0.2}\text{Mn}_{0.6}\text{Zr}_{0.2}\text{O}_{3-\delta}$  (0.1, 0.2, 0.25, 0.3). First, we report on how the crystal structure and the electrical properties of the two material systems change with Sr-content. Moreover, the study explores how Zr-substitution effects on oxygen vacancy ordering and optimization of the electrical properties through tuning of oxygen vacancy concentration and the oxidation states of Fe and Co.

## 2. Experimental

Solid solutions of the two series  $\text{La}_{1-x}\text{Sr}_x\text{Co}_{0.2}\text{Fe}_{0.6}\text{Zr}_{0.2}\text{O}_{3-\delta}$  (0.1–1.0) and  $\text{La}_{1-x}\text{Sr}_x\text{Co}_{0.2}\text{Mn}_{0.6}\text{Zr}_{0.2}\text{O}_{3-\delta}$  (0.1, 0.2, 0.25, 0.3) were prepared using a solid-state synthesis route. Stoichiometric amounts of  $\text{La}_2\text{O}_3$  (Sigma Aldrich, >99.99%),  $\text{SrCO}_3$  (Sigma Aldrich, >99.9%),  $\text{Co}_3\text{O}_4$  (Sigma Aldrich, >99.9%),  $\text{ZrO}_2$  (Sigma Aldrich, >99.9%),  $\text{Fe}_2\text{O}_3$  (Sigma

\* Corresponding author.

E-mail address: [vegar.oygarden@gmail.com](mailto:vegar.oygarden@gmail.com) (V. Øygarden).

Aldrich, >99.9%) and  $\text{MnO}_2$  (Sigma Aldrich, >99.9%) were mixed in 100% ethanol and ball milled at 60 rpm for 24 h.  $\text{La}_2\text{O}_3$  was dried at 800 °C overnight prior to use. 250 mL plastic bottles were used with the grinding media occupying between 1/3 and 1/2 of the bottle volume. The grinding media were balls of zirconia ceramics with 5 mm diameter. The ground powder mixtures were calcined at 1000–1100 °C for 12 h, and sieved through a 250  $\mu\text{m}$  mesh. Dense materials were obtained by uniaxial pressing (20 MPa) the powders into the desired shape, followed by heat treatment at 1350–1450 °C in air for 6 h to achieve densities greater than 93% of theoretical density with grain sizes in the range of 1–20  $\mu\text{m}$ .

The X-ray powder diffraction patterns were collected using a Bruker D5005 A-unit equipped with Cu-radiation and a primary monochromator. Data was collected from 15 to 130° with step size 0.012° and counting time 8 s per step. The diffraction patterns were fitted in Topas v4.2 using a Thompson-Cox-Hastings pseudo-Voigt peak model and Chebyshev background model with 5 orders.

Electronic conductivity was determined using a four-point DC method on densely sintered rectangular bar samples sized 5 × 10 × 50 mm. Constant current of 0.1 A was used on all samples. The samples were measured in two consecutive runs from room temperature to 1000 °C. The area specific resistance (ASR) of  $\text{La}_{1-x}\text{Sr}_x\text{Co}_{0.2}\text{Fe}_{0.6}\text{Zr}_{0.2}\text{O}_{3-\delta}$  ( $x = 0.5, 0.7$ ) was measured using high-temperature electronic impedance spectroscopy on symmetrical cells. A densely sintered sample of  $\text{Ce}_{0.9}\text{Gd}_{0.1}\text{O}_{2-\delta}$  was used as electrolyte, and the cathode materials were sprayed onto the electrolyte using a Sono-Tek spray coater equipped with a heating plate set to 70 °C. An infusion rate of 0.3 mL/min was used to apply 50–200  $\mu\text{m}$  thick layers onto both sides of the electrolyte, before sintering the cell for 2 h at 1025 °C. The cells were mounted using the ProboStat™ sample holder setup for circular discs and the impedance signal was analysed using an Alpha-A High Performance Frequency Analyser from Novocontrol. A typical impedance measurement covered the frequency range from 1 MHz to 10 mHz. An Ac-amplitude of 50 mV was used throughout the experiments. The impedance was modelled to an equivalent circuit using the ZSimpWin v3.21 software.

The thermal expansion of the materials was determined using a Netzsch DIL 402C dilatometer in air. 10 mm long cylindrical samples with 5 mm diameter sintered in air were polished to ensure parallel ends. The instrument was calibrated using an aluminium reference sample of known length. The thermal expansion coefficient was extracted using the Proteus analysing software.

### 3. Results

The X-ray diffraction (XRD) patterns of the solid solution series  $\text{La}_{1-x}\text{Sr}_x\text{Co}_{0.2}\text{Fe}_{0.6}\text{Zr}_{0.2}\text{O}_{3-\delta}$  (LSCFZ) are presented in Fig. 1. The diffraction pattern of  $x = 0.1$  correlates to the  $a^*a^*c^+$  tilt system. The lack of intensity at the  $0kl$  ( $k = 2n + 1$ ) reflections meant the material could be indexed to the orthorhombic  $Pbnm$  space group. The superreflections stemming from the orthorhombic superlattice are shown in the figure. The odd-odd-odd (R-point reflections) and even-even-odd reflections (X-point reflections stemming from simultaneous presence of both M- and R-points) decrease in intensity with increasing  $x$ . The R- and X-point reflections are no longer present for  $x = 0.3$ , although the 103 reflection is still observable. The absence of other superreflections suggests a higher symmetry orthorhombic or tetragonal structure such as  $lbmm$  (No. 74),  $P4/mbm$  (No. 127) or  $I4/mcm$  (No. 140). The Rietveld refinement gave the best fit to orthorhombic  $lbmm$ , but neutron diffraction or synchrotron X-ray diffraction data would be needed to determine the space group unambiguously. For  $x = 0.6$ , the intensity of the 103 diffraction peak is no longer present, and the material is indexed to cubic  $Pm\bar{3}m$ . The lattice parameters are summarised in Table 1.

The pseudocubic lattice parameters of LSCFZ are presented in Fig. 2. The unit cell parameters decrease with increasing Sr-content for  $x = 0.1$

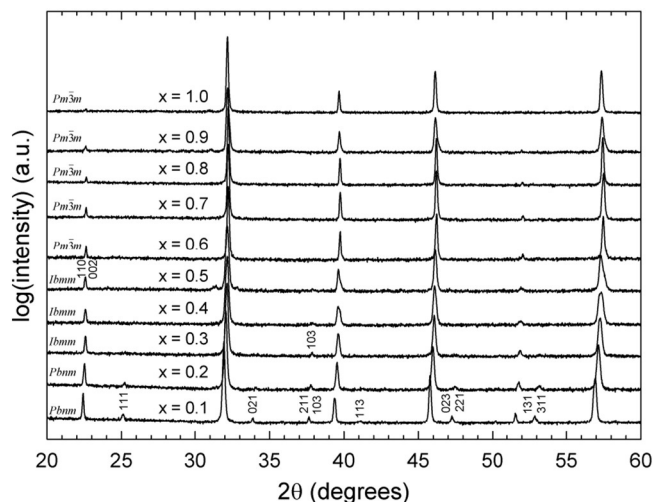
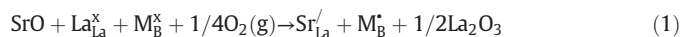
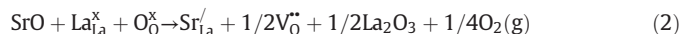


Fig. 1. X-ray diffraction patterns of  $\text{La}_{1-x}\text{Sr}_x\text{Co}_{0.2}\text{Fe}_{0.6}\text{Zr}_{0.2}\text{O}_{3-\delta}$  ( $0.1 \leq x \leq 1.0$ ). The superreflections stemming from orthorhombic  $Pbnm$  and  $lbmm$  symmetry are highlighted.

to  $x = 0.6$ . The unit cell volume of  $x = 0.7$  is similar to  $x = 0.6$ , and for higher values of  $x$ , the unit cell volume increases. The initial decrease of the unit cell is due to oxidation of Fe and Co as  $\text{La}^{3+}$  is substituted by  $\text{Sr}^{2+}$ , as described using Kröger-Vink notation [13] in Eq. (1).



Upon further Sr-substitution, the oxidation state of Fe and Co reaches a critical value where it is energetically more favourable to form oxygen vacancies rather than further oxidation of Co/Fe according Eq. (2). The increase in lattice volume seen in Fig. 2 for  $x > 0.7$  is due to the larger ionic size  $\text{Sr}^{2+}$  (1.40 Å) compared to  $\text{La}^{3+}$  (1.36 Å).



Any further Sr-substitution after this point will further increase the oxygen vacancy concentration. The concentration of oxygen vacancies is highly  $p\text{O}_2$ -dependent, which is made evident by re-heating  $x = 0.9$  in oxygen at 800 °C. As seen in Fig. 3, the unit cell parameters and volume decrease significantly as the material was oxidised at 800 °C.

The electrical conductivity of LSCFZ is presented in Fig. 3. The conductivity increases with increasing Sr-substitution up to  $x = 0.5$ , after which further substitution decreases the conductivity, in line with previous reports of similar systems.  $x = 0.1$  and  $0.2$  demonstrate semiconducting charge transport in the entire temperature interval, while the materials from  $x = 0.3$  to  $x = 1$  exhibit an apparent, gradual change from a semi-conductor to an apparently metallic behaviour. For  $x = 1$ , the change in the slope is seen at ~400 °C while at higher temperatures the materials appear to revert back to semiconducting behaviour as an increase in conductivity is seen with increasing temperature at high temperatures. No data was recorded for  $x = 1$  above ~850 °C due to sample-detachment. Table 1 summarises the conductivity at 700 °C for all the materials.

Fig. 4 shows the electrical conductivity plotted in isotherms from 400 to 900 °C as a function of Sr-content. The maximum conductivity is found for  $x = 0.5$  for all isotherms. The insert in Fig. 4 presents the temperature at which the slope of conductivity versus temperature changes sign. The transition temperature decreases roughly linearly as a function of Sr-content before it increases for  $x = 0.9$  and  $x = 1$ . This is related to the increased unit cell volume due to the increased concentration of oxygen vacancies as described earlier.

The area specific resistance (ASR) of the two most promising materials LSCFZ ( $x = 0.5$  and  $0.7$ ) was collected by high-temperature

Download English Version:

<https://daneshyari.com/en/article/5150505>

Download Persian Version:

<https://daneshyari.com/article/5150505>

[Daneshyari.com](https://daneshyari.com)